

Sequential Infiltration Synthesis for the Design of Low Refractive Index Surface Coatings with Controllable Thickness

1 Diana Berman,*§ Supratik Guha,‡,|| Byeongdu Lee,§ Jeffrey W. Elam,† Seth B. Darling,‡,||
 2 and Elena V. Shevchenko*,‡,||
 3

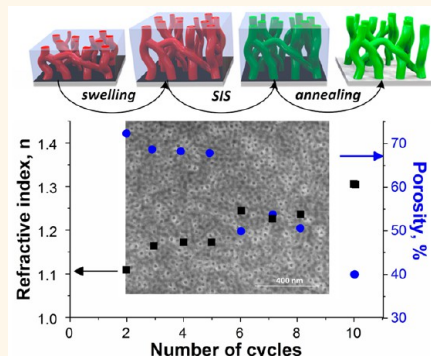
4 [‡]Center for Nanoscale Materials, [†]Energy Systems Division, and [§]Advanced Photon Source, Argonne National Laboratory, Argonne,
 5 Illinois 60439 United States

6 [§]Materials Science and Engineering Department, University of North Texas, Denton, Texas 76203 United States

7 ^{||}Institute for Molecular Engineering, University of Chicago, Chicago, Illinois 60637 United States

10 Supporting Information

11 **ABSTRACT:** Control over refractive index and thickness of surface coatings is
 12 central to the design of low refraction films used in applications ranging from
 13 optical computing to antireflective coatings. Here, we introduce gas-phase
 14 sequential infiltration synthesis (SIS) as a robust, powerful, and efficient
 15 approach to deposit conformal coatings with very low refractive indices. We
 16 demonstrate that the refractive indices of inorganic coatings can be efficiently
 17 tuned by the number of cycles used in the SIS process, composition, and
 18 selective swelling of the polymer template. We show that the refractive
 19 index of Al_2O_3 can be lowered from 1.76 down to 1.1 using this method. The
 20 thickness of the Al_2O_3 coating can be efficiently controlled by the swelling of the
 21 block copolymer template in ethanol at elevated temperature, thereby enabling
 22 deposition of both single-layer and graded-index broadband antireflective
 23 coatings. Using this technique, Fresnel reflections of glass can be reduced to as
 24 low as 0.1% under normal illumination over a broad spectral range.



25 **KEYWORDS:** antireflective, sequential infiltration synthesis, block copolymer, porous, low refractive index, polymer swelling

26 **A** broad array of applications ranging from high-
 27 performance computing to antireflective coatings can
 28 benefit from the ability to manipulate refractive index in
 29 thin films. The refractive index of surface coatings is determined
 30 by a combination of composition and structure. The availability
 31 of materials with suitable refractive indices, especially for optical
 32 applications, is limited. Coatings with low refractive indices
 33 improve the performance of light emitting diodes, solar cells,
 34 and eye glasses.¹ Materials with refractive indices below 1.20 are
 35 highly desired for distributed Bragg reflectors used in
 36 waveguides and other high-performance optics; however,
 37 dense materials with such low refractive indices do not exist.
 38 The reduction of light reflected off surfaces relies on adjusting
 39 both the thickness and refractive index of the antireflective
 40 coating (ARC) in a way that the light reflected off two
 41 interfaces, such as air/coating and coating/substrate, interferes
 42 destructively. According to the Fresnel equation, this condition
 43 can be achieved for a given wavelength λ and angle of incidence
 44 when the thickness of the ARC is $\sim\lambda/4$ and refractive index of
 45 the ARC equals the square-root of the substrate refractive
 46 index. The ability to lower the refractive index of the materials
 47 is critical for the design of ARCs that help to minimize the

48 reflection of the light and improve efficiency. For example, an ARC of MgF_2 on the surface of float glass can decrease the 49 amount of the reflected light from 4.3% to almost 1% at the 50 specified center wavelength and normal incidence, thereby 51 increasing transmission in a given spectral range.²

52 ARCs on the surfaces of materials with relatively low 53 refractive indices, such as fused glass (1.458), crown glass 54 (1.485), sapphire glass (1.768), Gorilla glass (1.5), and 55 polycarbonate (1.586) are of particular interest for corrective 56 lenses, telescopes, and flat-panel displays. In telescopes that 57 typically have several optical components, additive energy loss 58 of reflected light can be substantial, hence effective ARCs are 59 required. ARCs on flat-panel displays of electronic devices help 60 eliminate stray reflections that cause unwanted veil glares. 61 Single-layer MgF_2 (with a refractive index of 1.38) is the most 62 commonly used ARC for surfaces with low refractive index. 63 Even though its performance is not exceptional, it still provides 64

Received: December 13, 2016

Accepted: January 31, 2017

Published: January 31, 2017

65 decent antireflective properties in the middle of the visible band
66 and works reasonably well for the entire spectral range.³ Better
67 performing ARCs for surfaces with low refractive indices
68 typically consist of several metal oxide layers (e.g., TiO₂, ITO,
69 etc.), SiO₂, and polymers.⁴ While one's ability to prepare high
70 refractive index coatings is limited by the nature of available
71 materials, the refractive index of optical films can be lowered by
72 inducing suboptical porosity. For example, the refractive index
73 of bulk silica (SiO₂) is 1.46; however, nanoporous SiO₂ films
74 with refractive index of 1.08 have been reported,⁵ which
75 represents a value far below the lowest refractive index known
76 for dense inorganic materials, such as 1.38 for MgF₂.⁶ Widely
77 used conventional single-layer ARCs target only a particular
78 wavelength at normal incidence, while graded-index coatings
79 allow omnidirectional broadband properties.⁷ ARCs can be
80 deposited (i) chemically, for example, by spin-casting of silica
81 sols⁸ or by layer-by-layer (LBL) deposition of charged colloids
82 and polymers,^{9,10} (ii) using vacuum-based coating techniques,⁷
83 or (iii) by texturing the surface using lithographic and chemical
84 approaches (e.g., *via* etching).^{11–15} These methods allow
85 synthesis of porous films with different degrees of control
86 over the film porosity. Since polymers are typically less stable
87 against heat and UV light compared to inorganic materials,¹⁶
88 porous inorganic coatings are preferred for a broad range of
89 applications. When employing chemical approaches, the
90 porosity of inorganic films can be tuned mainly by the size of
91 the particles in the deposited nanoparticle arrays or by the size
92 of the introduced polymeric fillers that are subsequently
93 removed by solvent treatment or oxidative annealing.¹⁷
94 Chemical approaches are straightforward for single-layer
95 ARCs; however, they do not work well for graded-index
96 coatings. Also, chemical deposition efforts have largely focused
97 on silica coatings, which limits the control over the refractive
98 index. Physical vapor deposition performed at a glancing angle
99 yields nanostructured films with controllable porosity as a result
100 of the self-shadowing effect and surface diffusion.¹⁸ This
101 technique has achieved the record low refractive index of 1.05.⁷
102 In vacuum methods, graded-index ARCs are obtained *via*
103 deposition of a number of layers with different porosity and
104 composition. Such methods are usually applied for ARCs on
105 small area surfaces due to their high cost of fabrication.

106 In general, the tuning of the refractive index of ARCs is a
107 labor-intensive process, both in physical and chemical
108 approaches. Lithographic and physical methods can produce
109 ARCs with finely tuned refractive indices, resulting in excellent
110 optical performance, however, this is achieved at the expense of
111 high cost. In turn, the cost of chemically fabricated ARCs is
112 reasonable; however, their performance is somewhat compro-
113 mised, mainly because of the inability to finely control the
114 refractive index. Design of multilayered ARCs by chemical
115 methods, such as sol–gels, dipping or spinning processes, is
116 challenging since each layer requires thermal annealing that can
117 alter the porosity in the previously deposited layers affecting
118 their optical properties. Also, chemical methods based on
119 etching are not well suited to fabricate gradient structures due
120 to potential impact of the etching agents on structures
121 fabricated in the previous steps. However, the biggest challenge
122 for ARCs on surfaces with low refractive indices is that
123 regardless of the fabrication method, state-of-the-art graded-
124 index ARCs on surfaces with low refractive indices assume the
125 initial deposition of coatings with high refractive indices. This
126 step of artificial increase of refractive index of the surface is

needed since there is only a limited number of materials (and
127 approaches leading to materials) with refractive index <1.5.
128

Here we propose an efficient combined chemo-physical
129 approach to finely control refractive index that can be used for
130 single-layer and graded-index surface ARC coatings. The
131 strategy is based on sequential infiltration synthesis (SIS),
132 which involves diffusion-controlled penetration and subsequent
133 chemisorption of inorganic precursor molecules inside a
134 polymer template. In SIS, the precursors are introduced to
135 the substrate in the vapor phase. Following SIS, the polymer
136 matrix is removed *via* thermal annealing. When using block
137 copolymer (BCP) films as substrates for SIS, one can achieve
138 growth of the inorganic phase selectively within one of the
139 polymer blocks. In this way, the self-assembled nanostructures
140 of the BCP can be replicated in a functional, inorganic material.
141 As SIS is diffusion controlled, growth within thick films can be
142 cumbersome with difficult to predict reaction kinetics.¹⁹ In this
143 study, we report that swelling of the block copolymer template
144 in ethanol at different temperatures prior to SIS efficiently
145 tunes the thickness and porosity of the resulting ARCs and
146 enables the fabrication of optical surface coatings for a desired
147 spectral range. Solvent-assisted SIS can also produce multi-
148 layered graded index structures to deposit broadband ARCs.
149 We believe the solvent-assisted SIS approach offers an
150 opportunity to eliminate the commonly accepted artificial
151 increase of surface refractive index in broadband multilayered
152 ARCs for the materials with low refractive indices.
153

RESULTS AND DISCUSSION

When SIS is performed on a polymer such as poly(methyl
155 methacrylate) (PMMA), the vapors of the inorganic precursor
156 molecules infiltrate the bulk of the film and react with C=O
157 and –C–O–R functional polar groups of the polymer
158 macromolecule.^{19–21} In the case of diblock copolymers with
159 a purely hydrocarbon block, such as polystyrene (PS),
160 connected to a block exhibiting polar groups (e.g., PS-*b*-
161 PMMA), the overall molecular weight and the volume fractions
162 of the two blocks determine the morphology and size of the
163 nanoscopic domains, which serve as a template for the SIS
164 processed material. Earlier studies demonstrated that SIS in
165 diblock copolymer films is a strategy to synthesize nanophase
166 inorganic materials and to improve the quality of litho-
167 graphically prepared features.^{22,23} However, the optical proper-
168 ties of SIS-modified diblock copolymers have not yet been
169 explored.
170

In this work, we demonstrate the ability to tune refractive
171 indices by SIS and utilize this capability to synthesize
172 antireflective coatings. We studied two types of block
173 copolymers, polystyrene-*b*-poly(methyl methacrylate) (PS-
174 *b*-PMMA) and poly(styrene-*b*-4-vinylpyridine) (PS-*b*-
175 P4VP), as templates for SIS of inorganic materials with tunable
176 refractive indices and antireflective properties.
177

PS-*b*-PMMA is one of the most popular BCPs and is
178 frequently used in SIS.^{20,24–26} PS-*b*-PMMA has been used as a
179 template to pattern ZnO, Al₂O₃, SiO₂, TiO₂, W and other
180 materials with different degrees of control over periodicity and
181 structure.^{19–21,27} Al₂O₃ SIS, in particular, has a robust
182 chemistry with well-understood kinetics. Thus, we chose PS-
183 *b*-PMMA-templated Al₂O₃ SIS as a model system for this study.
184 Spin-casting 2 wt % toluene solutions of PS-*b*-PMMA with
185 different percentage of PS followed by 1 h thermal annealing in
186 argon atmosphere at 180 °C resulted in uniform, 70 ± 5 nm-
187 thick films with microphase-separated domains. Since the long-
188

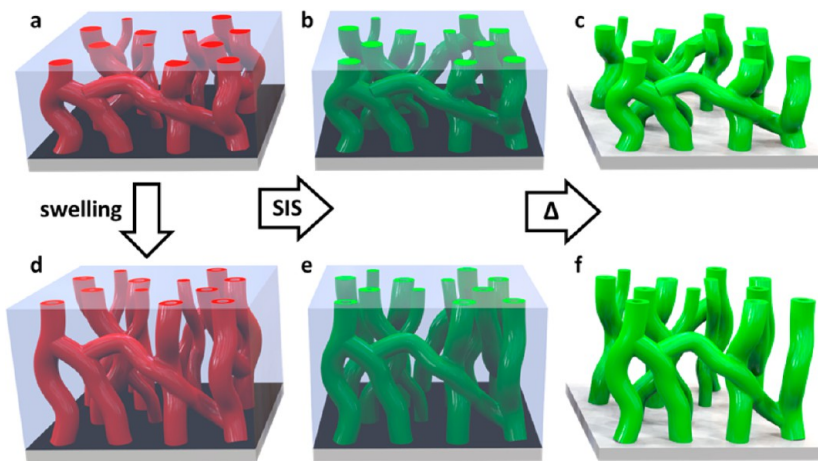


Figure 1. Depiction of the SIS (a–c) and solvent-assisted SIS (d–f) procedures leading to formation of porous Al_2O_3 coatings. Hydrophilic polymer domains (e.g., PMMA or P4VP, shown in red) are infiltrated with the precursor of Al_2O_3 (shown in green) and converted into porous Al_2O_3 upon oxidative annealing.

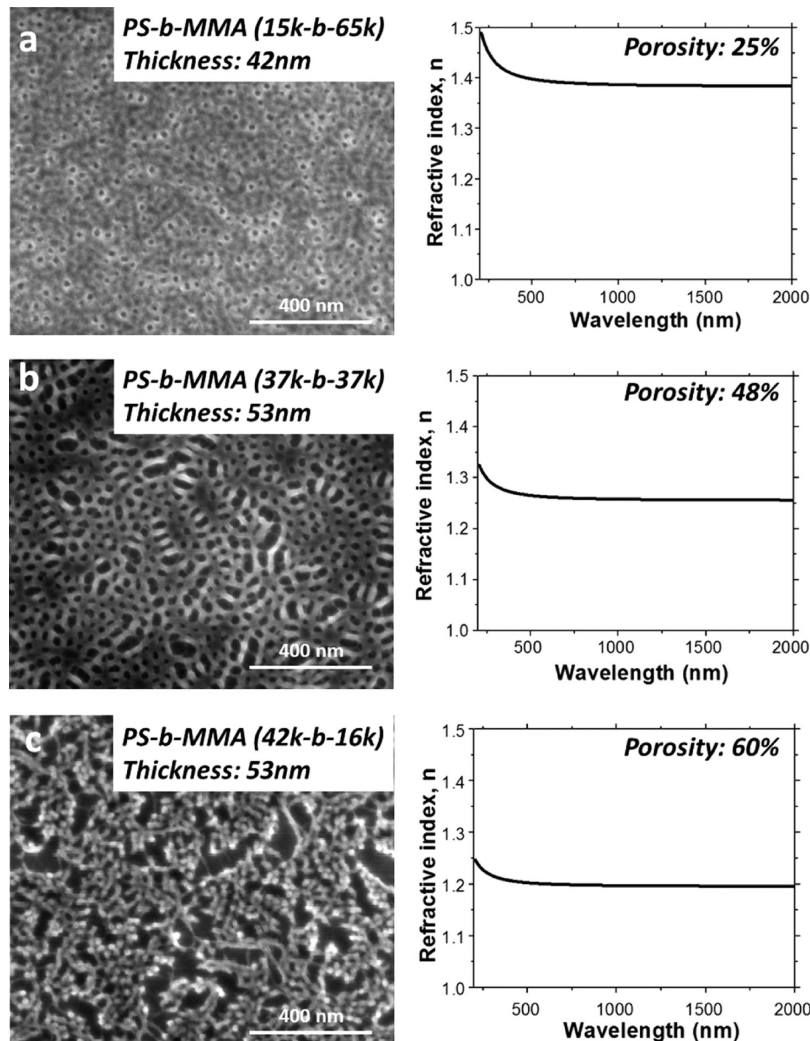


Figure 2. SEM images and the corresponding refractive indices of porous alumina films grown by the infiltration (5 SIS cycles) of PS-*b*-PMMA polymers with different volume fraction of polystyrene: (a) 15k-*b*-65k, (b) 37k-*b*-37k, and (c) 42k-*b*-16k.

189 range periodicity of structures at a scale far below the
190 wavelength of visible light is not expected to affect the
191 refractive index of the material, we did not perform additional
192 procedures to induce long-range orientational order.^{28,29}

Stepwise exposure of PS-*b*-PMMA to vapors of trimethylaluminum (TMA) and water during 5 cycles of SIS led to the 194 growth of Al_2O_3 within the PMMA domains. Next, the polymer 195 template was removed by oxidative thermal annealing for 1 h at 196 f°

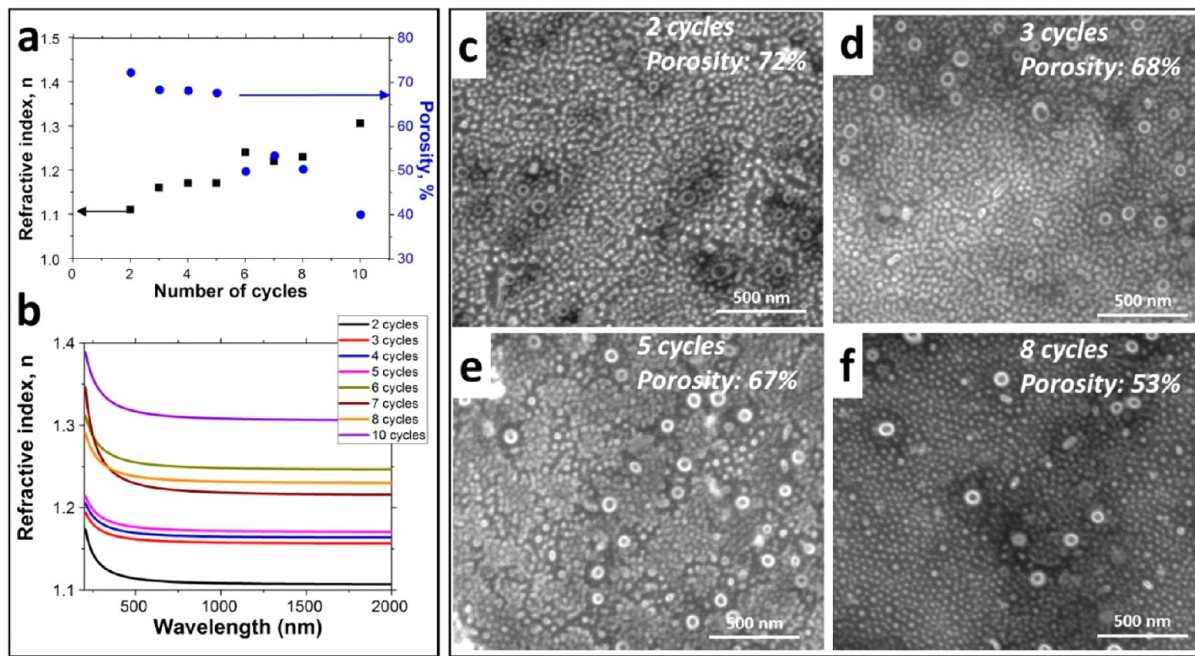


Figure 3. Porous alumina films grown by the infiltration of PS-*b*-P4VP with TMA/water as a function of number of SIS cycles. (a) Refractive indices measured at 785 nm wavelength and porosity show variation with the number of cycles. (b) Refractive index values *vs* wavelength for films obtained with different numbers of SIS cycles. (c) Representative SEM images of the grown Al₂O₃ films demonstrate evolution of the material structure as a function of the SIS cycle number. The thickness of the films shown in (c–f) is 48.7 ± 5.1 nm.

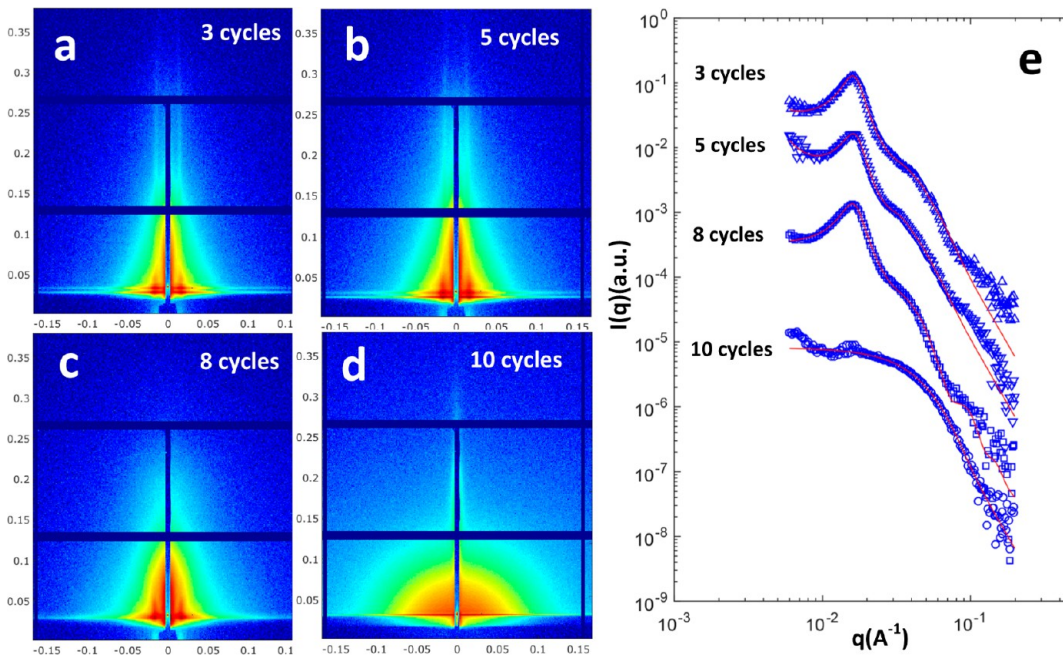


Figure 4. GISAXS (a–d) and transmission SAXS (e) data and fit (solid red line) for Al₂O₃ SIS films obtained with different number of SIS cycles. In (e), the data are arbitrarily scaled for better visualization.

197 450 °C. Figure 1 captures the processes involved in the
198 formation of porous metal oxide films by infiltration of
199 polymers without (a–c) and with swelling (d–f). The oxidative
200 annealing of the SIS films proved to be more efficient than
201 either ozone or plasma etching, which resulted in bubbling and
202 rupture of the Al₂O₃ films due to rapid release of CO₂ (Figure
203 S1).

204 Figure 2 shows SEM images of thin Al₂O₃ films with a
205 different degree of porosity controlled by the PS/PMMA ratio

206 on a silicon surface. Ellipsometry reveals that refractive indices
207 are inversely proportional to the porosity and vary from 1.2 at
208 60% porosity to 1.39 at 25% porosity at a wavelength of 785
209 nm. These values are far below the 1.768 value characteristic to
210 bulk alumina and also significantly below the value of 1.6 for
211 amorphous ALD Al₂O₃.³⁰ Thus, we have demonstrated tuning
212 of refractive indices of Al₂O₃ SIS films and satisfied one
213 criterion for design of ARCs. The thickness of these films was
214 not sufficient to provide antireflective properties to the coatings
215

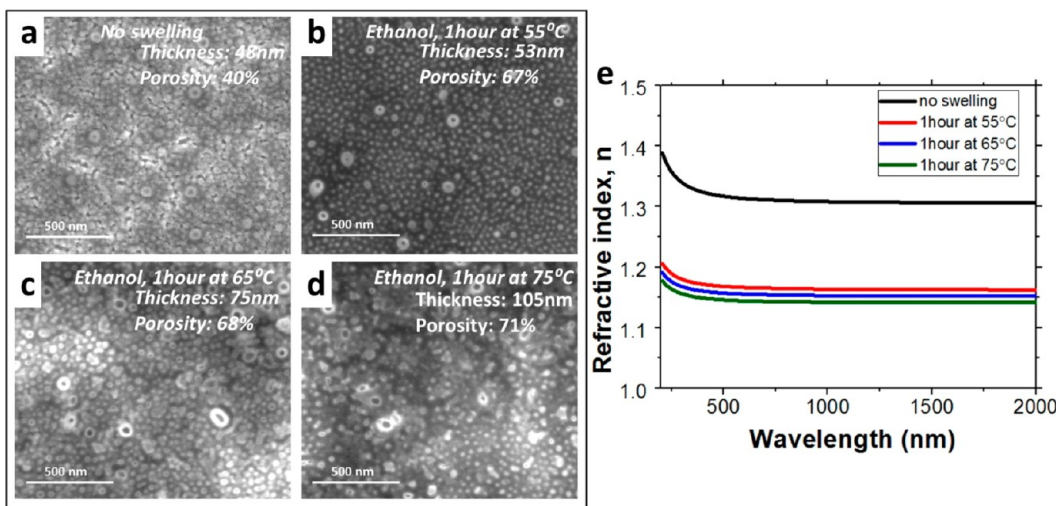


Figure 5. Porous alumina films grown by the infiltration of PS-*b*-P4VP polymers (10 cycles) without swelling in ethanol (a) and after swelling for 1 h at different temperatures at 55 °C (b), 65 °C (c), and 75 °C (d). The refractive indices of alumina films obtained with no polymer swelling and as different swelling regimes (e).

215 in the spectral range above 200 nm. Increase in the thickness of
216 the PS-*b*-PMMA template achieved by increase of the
217 concentration of the polymer in toluene solution did not lead
218 to thicker final Al₂O₃ films, likely due to limited diffusion of
219 TMA through the as-deposited film under these SIS conditions.
220 Swelling of BCPs in certain solvents was previously reported
221 to induce porosity that potentially could assist the growth of
222 thicker SIS films.³¹ Swelling of our polymer templates with
223 acetic acid, a procedure that worked well for periodic pre-
224 aligned PS-*b*-PMMA,³¹ was found to be partially successful.
225 Acetic acid swelling allowed us to increase the overall thickness
226 of the Al₂O₃ SIS films; however, the films were laterally non-
227 uniform and were rather rough. In an effort to integrate
228 swelling-induced porosity with a more controllable morphol-
229 ogy, we turned our attention to another polymer system, PS-*b*-
230 P4VP, as this is a model system for studying swelling
231 phenomena in polymers.³²

232 First, we conducted the set of experiments to confirm that
233 PS-*b*-P4VP would work as an efficient template for deposition
234 of alumina by SIS. We used a 2 wt % of PS-*b*-P4VP (75k-*b*-25k)
235 BCP solution in toluene to spin-cast 80 nm-thick polymer
236 templates and successfully obtained porous Al₂O₃ with
237 refractive indices in the range between 1.11 and 1.25 following
238 Al₂O₃ SIS and heat treatment procedures (Figure 3). We found
239 that the porosity could be tuned by adjusting the number of SIS
240 Al₂O₃ cycles. In particular, the porosity decreased monotonically
241 with the number of SIS Al₂O₃ cycles. Dispersion of feature
242 sizes in the Al₂O₃ SIS films prepared using PS-*b*-P4VP is a
243 result of polydispersity present in the BCP material (most likely
244 due to the presence of homopolymer) causing some size
245 distribution of P4VP domains. The thickness of the alumina
246 films produced by SIS, as measured by ellipsometry, was 48.7 ±
247 5.1 nm.

248 Grazing incidence small-angle X-ray scattering (GISAXS)
249 patterns of samples prepared with 3 and 5 SIS cycles are similar
250 (Figure 4). Both patterns presented a peak at $q_y = 0.0165 \text{ \AA}^{-1}$,
251 indicating 2D nanostructures laterally ordered with a *d*-spacing
252 of ~38 nm. GISAXS pattern obtained for the sample with 3 SIS
253 cycles allowed for estimation of the thickness of the Al₂O₃ film
254 as ~45 nm, which is in agreement with the ellipsometry data
255 (Table S1). The shape of the peaks is generally a circular spot

256 along the vertical direction, indicating that the lateral structure
257 is as tall as the film thickness, although the peaks' weak vertical
258 tails suggest coexistence of smaller features. The vertical sizes of
259 the smaller features ranged from 5.0 to 6.0 nm and increased
260 slightly with the number of SIS cycles. These values, obtained
261 by fitting the data to a polydisperse sphere model, are
262 summarized in Table S1. We also found at least two feature
263 sizes along the horizontal direction, which are about 25 and 10
264 nm, respectively. These scattering results suggest that Al₂O₃
265 pillars seen in Figure 3 are made of smaller Al₂O₃ grains. After
266 10 SIS Al₂O₃ cycles, the sample completely lost lateral ordering
267 peaks, and only randomly distributed spherical 8 nm particles
268 are observed, indicating that the Al₂O₃ particles are probably
269 grown on the surface of the polymer film. Electron densities
270 obtained from the GISAXS patterns^{33,34} are 0.243, 0.214, 0.403,
271 and ~0.7 e/Å³ for Al₂O₃ SIS films obtained with 3, 5, 8, and 10
272 SIS cycles, respectively. Considering the electron density of
273 Al₂O₃ is 1.17 e/Å³, their porosities of 2–5, 8, and 10 SIS cycles
274 are 80, 65, and 40%, respectively. The summary of the GISAXS
275 and SAXS data is given in Table S1. Ellipsometry measure-
276 ments estimated the porosity of the same structures as 68, 58,
277 and 40%, which is in relatively good agreement with SAXS data.
278

279 We have demonstrated that Al₂O₃ SIS in PS-*b*-P4VP
280 templates yields even lower refractive indices values compared
281 to PS-*b*-PMMA. However, as in the case of PS-*b*-PMMA,
282 increasing the thickness of the PS-*b*-P4VP template did not
283 increase the resulting Al₂O₃ film thickness beyond ~48 nm,
284 which again relates to slow diffusion of the TMA precursor
285 through the free volume of the PS-*b*-P4VP film. In order to
286 introduce porosity to enhance diffusivity, we explored swelling.
287 Swelling is a nondestructive strategy to induce and modify the
288 porosity in BCP materials.³¹ It is performed by immersing the
289 BCP film in a solvent that is selective to the minority block.
290 Upon drying, pores are generated throughout the film in the
291 positions where the minority block has collapsed. Swelling of
292 PS-*b*-P4VP in ethanol at different temperatures allows the
293 formation of interconnected pores in the range between 10 and
294 50 nm.³¹ These pores are much larger than the molecular-scale
295 pores that define the polymer-free volume. Given that Knudsen
296 diffusion scales as the diameter squared,³⁵ we expect a much
297 more rapid and effective infiltration of the TMA into the
298

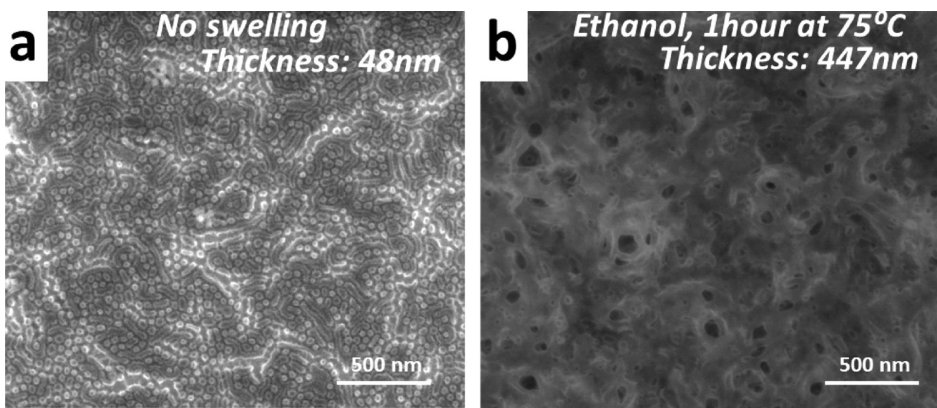


Figure 6. Porous alumina films grown by the infiltration during 5 SIS cycles of spin-cast 400 nm-thick PS-*b*-P4VP polymer (75k-*b*-25k) templated without swelling (a) and (b) after swelling at 75 °C for 1h.

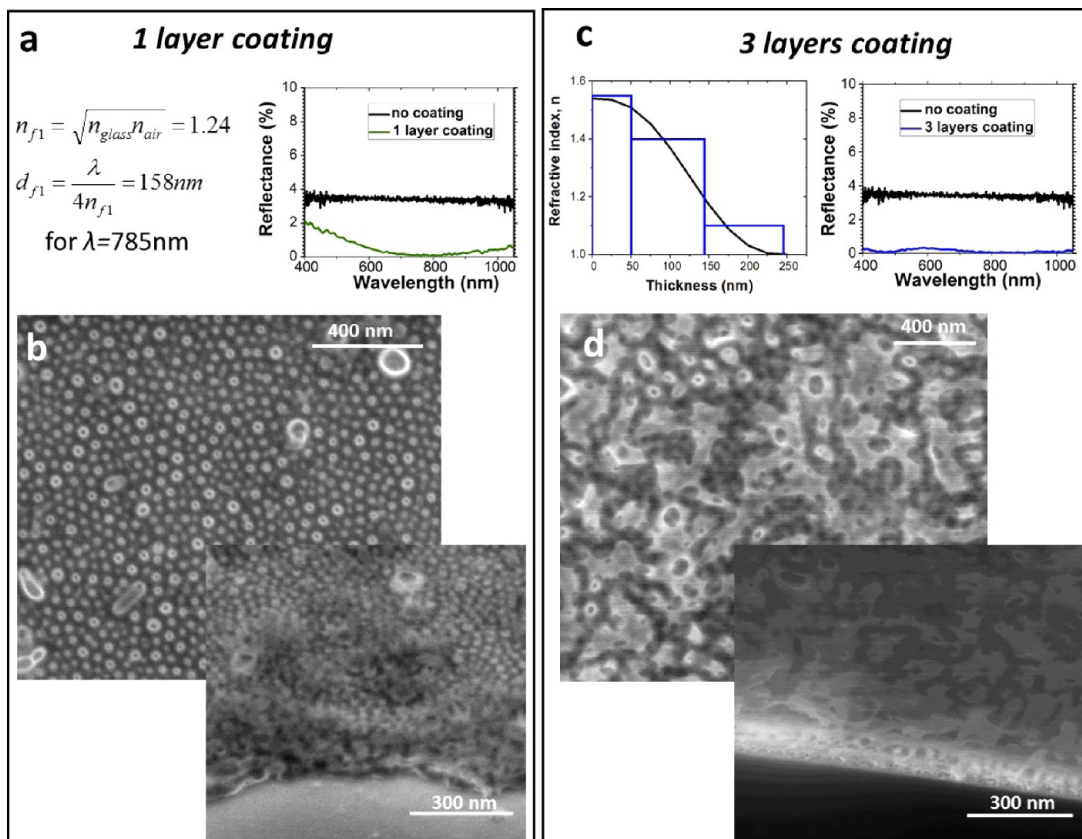


Figure 7. Two cases of antireflective coatings with single wavelength minimized reflection (a,b) and wide range minimized reflection deposited on the glass substrate (c,d). Figures (b) and (d) demonstrate the SEM images of porous Al₂O₃ coatings on silicon substrate fabricated by solvent-assisted SIS technique using the same synthesis parameters that were used for deposition on a glass substrate. Porous Al₂O₃ film deposited on glass with the use of PS-*b*-P4VP (75k-*b*-25k) precursor demonstrates minimized reflection for 785 nm light in comparison to bare glass (a); a three-layer Al₂O₃ deposited on glass in sequence with the assistance of three different polymer films demonstrates reduced reflection over the broad wavelength range of 400–1050 nm (c).

297 solvent-treated PS-*b*-P4VP films compared to the untreated
298 films.

299 We immersed 80 nm-thick PS-*b*-P4VP films for 1 h in
300 ethanol at different temperatures. After drying the samples
301 under dry nitrogen for 10 min to remove excess ethanol, the
302 Al₂O₃ SIS was performed. We increased the number of SIS
303 cycles to 10 in order to target thicker films. Figure 5a
304 demonstrates that Al₂O₃ SIS films prepared with 10 SIS cycles
305 are still porous but rather dense. The porosity of the film
306 estimated by ellipsometry is ~40%, which is in a good
307

308 agreement with SAXS data (Figure 4e). Figure 5b–d shows
309 that swelling of the PS-*b*-P4VP template at different temper-
310 atures increases the porosity of the Al₂O₃ films, resulting in
311 substantially lower refractive indices (Figure 5e). More
312 importantly, the polymer swelling also yielded thicker Al₂O₃
313 SIS films. Figure 1 depicts the effect of swelling on the
314 morphology of the final Al₂O₃ films. The Al₂O₃ films prepared
315 using an untreated 80 nm-thick PS-*b*-P4VP template were only
316 ~48 nm in thickness. However, swelling the 80 nm-thick PS-*b*-
317 P4VP template films in ethanol at temperatures of 55, 65, and
318

317 75 °C yielded Al_2O_3 film thicknesses of 53, 75, and 105 nm,
318 respectively. We attribute this increase in thickness to the more
319 effective diffusion of TMA through the 10–50 nm void spaces
320 remaining after removing the PS component of the polymer
321 template films.

322 The refractive indices of the Al_2O_3 SIS films obtained at
323 different swelling temperatures were in the range between 1.17
324 and 1.14. These values are far below the lowest refractive index
325 known for bulk inorganic materials such as the widely used
326 MgF_2 in the design of ARCs.³⁶ The swelling property of the
327 BCP is essential for the deposition of ARCs since it allows for
328 tuning the thickness of the surface coating, which is critical for
329 achieving a low reflectivity in a specific, targeted spectral range.
330 Figure 6 shows that swelling of a 400 nm-thick PS-*b*-P4VP film
331 in ethanol for 1 h at 75 °C leads to a 447 nm-thick porous
332 Al_2O_3 SIS film, while no swelling results in the thickness limited
333 by ~48 nm value (Figure 6a).

334 With control established over both the refractive index and
335 thickness of the deposited films, we proceeded to explore the
336 SIS process to prepare ARC coatings. For a single-layer ARC,
337 light reflection will be minimized when the coating satisfies
338 certain criteria for its refractive index and thickness. The
339 refractive index of the antireflection coating (n_{fl}) should be
340 $n_{\text{fl}} = \sqrt{n_s n_{\text{air}}}$, where n_s and n_{air} are the refractive indices of the
341 substrate and air, respectively. The optimum thickness of the
342 ARC (d_{fl}) should be $d_{\text{fl}} = \frac{\lambda_0}{4n_{\text{fl}}}$, where λ_0 is the wavelength of
343 the light to be fully transmitted. For example, in order to
344 eliminate the reflection of 785 nm wavelength light at a glass
345 substrate with refractive index of 1.54, an 158 nm-thick ARC
346 with refractive index of 1.24 is required. We prepared such an
347 Al_2O_3 SIS coating by spin coating 80 nm-thick PS-*b*-P4VP and
348 swelling it at 75 °C, followed by 10 SIS cycles. The thickness of
349 this coating was 152 ± 8 nm, and the refractive index was 1.24.
350 Reflectivity measurements indicate that only 0.1% of the light is
351 reflected at ~780 nm, while the uncoated glass substrate
352 reflected ~14% (Figure 7a). Figure 7a demonstrates that, in
353 fact, the deposited single-layer Al_2O_3 SIS coating lowered the
354 reflectivity in the entire 400–800 nm spectral range.

355 The main challenge for synthesis of ARCs that can eliminate
356 the Fresnel reflection over a broad spectral range is
357 unavailability of materials with very low refractive indices that
358 can closely match the refractive index of air. Light reflection is
359 minimized when the coating refractive index exhibits a
360 continuous gradient change along the thickness from the
361 value of the substrate material at the substrate/coating interface
362 down to the air refractive index at the coating/air interface.^{37–39} The deposition of films with uniform gradient change
363 is challenging. Previous studies have demonstrated dramatic
364 reduction in the light reflection for a coating made of several
365 discrete layers with different constant refractive indices.⁷
366 Control over the refractive index in graded-index structures
367 of this nature minimized reflectivity over a broad spectral
368 range.⁷ Previous studies demonstrated that this goal can be
369 achieved by deposition of layers of certain materials with
370 controlled thickness and porosity by oblique-angle deposition.
371 However, even though oblique-angle deposition obtained a
372 record low refractive index of 1.05 for multilayers of TiO_2 and
373 SiO_2 , it is challenging to use this method for larger scales.
374 We explored the potential of SIS to design graded-index
375 ARCs. To this end, we deposited three stacked layers of Al_2O_3
376 SIS films. Figure 7c shows the strategy we followed in terms of
377 parameters selected for each layer. In order to minimize the

378 reflectivity of the glass surface in spectral range 400–1050 nm,
379 a minimum of three layers with the following refractive indices
380 and thicknesses are required: 1.54 and 50 nm (first layer); 1.4
381 and 190 nm (second layer); and 1.1 and 200 nm (third layer).
382 First layer was obtained by SIS using 80 nm-thick PS-*b*-PMMA
383 and 10 SIS cycles. PS-*b*-P4VP templates of 80 nm and 10 and 5
384 SIS cycles, respectively, were used to form the second and third
385 layers. The first and second layers were annealed at 450 °C
386 under air flow for 1 h to remove the polymer prior to spin-
387 casting of the second and third layers of a polymer template,
388 correspondingly.

389 As evidenced from SEM imaging, the final film is porous and
390 rather uniform (Figure 7d). Wavelength dependence of
391 specular reflectivity demonstrated that the glass with three
392 layers of Al_2O_3 SIS coating reflects between 0.4% and 0.1% of
393 the light in the range of 400–1050 nm at normal incidence.
394 Photographs of the uncoated glass and glass with single and
395 multilayer coatings with optical characteristics are shown in
396 Figure 8. The blue background in the area covered by uncoated
397 glass is darker as compared with the uncovered area, whereas
398 there is no visually detectable difference in the color of the blue
399 background in the areas uncovered and covered with glass
400 substrates with single- and three-layered ARCs. In order to
401 quantify this observation, we analyzed the color of the images
402 shown in Figure 8a in the areas uncovered (n) and covered
403 with glass substrates (n*). We compared the color histograms
404 in the areas covered by coated glass within the neighboring
405 uncovered areas. Figure 8b demonstrates that the significant
406 shift toward the darker color is observed in the area covered by
407 plain glass, while a minor shift and no change in color
408 histogram are observed for one- and three-layer coatings,
409 respectively. These data indicate better light transmittance and
410 the absence of residual carbon in the thermally annealed films.
411 Energy dispersive X-ray analysis confirms that no carbon
412 remains in the thermally annealed samples (Figure S2). As
413 shown in Figure 8c, transmittance increased from ~92.5%
414 (uncoated glass sample) to ~96.5% in a narrow range around
415 785 nm for the single-layer coated sample. In the case of three-
416 layer films, the transmittance is improved to ~95% in the whole
417 visible light spectral range. Since the reflectance both in case of
418 single-layer and gradient coatings was found to be <1%
419 (Figures 7a and 7c), we attribute the losses in the transmittance
420 in the coated samples to the light scattering at the larger
421 features present in the Al_2O_3 (Figure 7b,d) formed as a result of
422 polydispersity and/or homopolymer present in the original
423 BCP template.

424 Contact angle measurements demonstrated that the Al_2O_3
425 SIS coatings rendered the glass surface more hydrophobic
426 (Figure 8c). The contact angle of water droplet at the surface of
427 uncoated glass was 32 ± 2 °. Deposition of single-layer Al_2O_3
428 SIS coating resulted in contacted angles of 42 ± 3 °. Three-layer
429 Al_2O_3 SIS coating demonstrated a contact angle of 57 ± 3 °.
430 This trend can be explained by increased porosity of the
431 surface.

CONCLUSIONS

432 In conclusion, low refractive index coatings can be successfully
433 obtained using gas-phase SIS. We have shown that the
434 refractive indices of inorganic coatings can be efficiently
435 tuned by the volume fraction of the SIS-binding block in the
436 BCP and by the number of SIS cycles. The refractive index of
437 Al_2O_3 can be lowered down to 1.1 by SIS. We have
438 demonstrated that the thickness of the Al_2O_3 surface coating
439

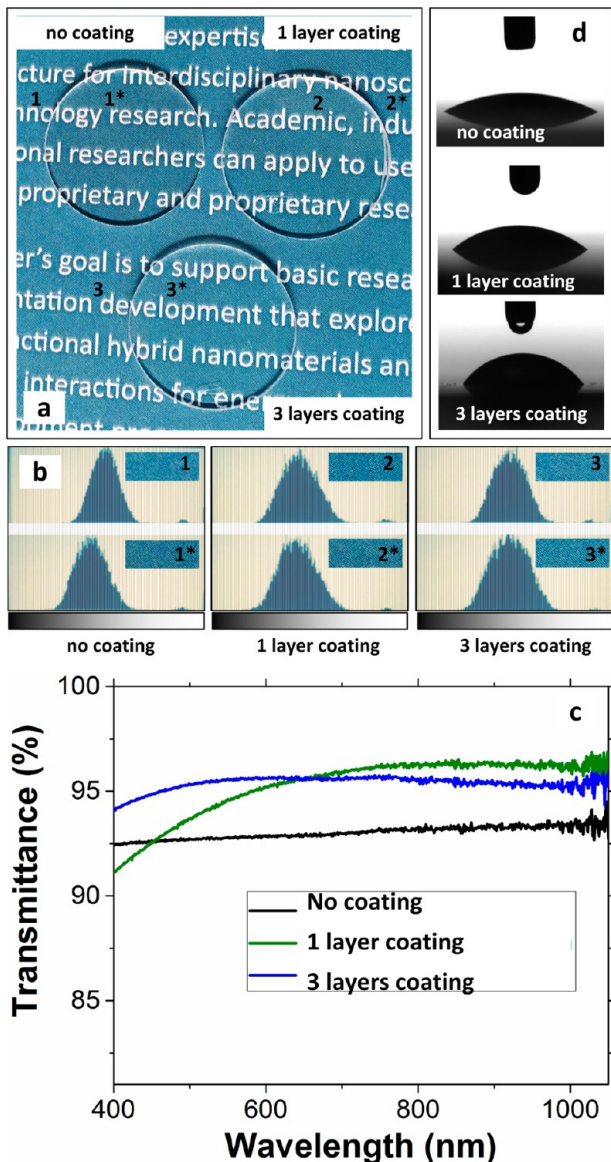


Figure 8. Photograph of uncoated glass and glass with single-layer and graded index ARCs (a). Color histograms (b) obtained for the selected areas of the blue background denoted in (a) as n and n^* . (c) Transmittance spectra of glass and glass samples coated with single- and gradient three-layers aluminum oxide. (d) Photographs demonstrating the contact angle of water droplet at the surface of plain glass and glass with single-layer and graded index ARCs.

can be efficiently controlled by solvent swelling of the template, which induces porosity in the BCP and, as a result, facilitates rapid diffusion for the precursor molecules and complete infiltration of the polymer film. Control over the thickness of the SIS coating has enabled the deposition of both particular spectral range and graded-index broadband ARCs. Fresnel reflections have been shown to decrease down to 0.1% under normal illumination over a broad spectral range. The deposition of low refractive index coating by SIS is simple and robust. Since porosity and thickness of the films can be efficiently tuned in a broad range, solvent-assisted SIS does not require an artificial increase of the refractive index of the low refractivity substrate surface as is commonly accepted in the design of broad band antireflective coatings. We believe that SIS can be easily applied to a broad range of materials and can be

considered as a cost-efficient alternative to the oblique-angle techniques currently used for deposition of broadband ARCs.

METHODS AND EXPERIMENTAL DETAILS

Materials. Two types of block copolymers used in the study, poly(styrene-block-4-vinylpyridine) (PS-*b*-P4VP) and polystyrene-*b*-block-poly(methyl methacrylate) (PS-*b*-PMMA) with different lengths of polar and nonpolar blocks (PS_{75k}-*b*-PMMA_{25k}, PS_{15k}-*b*-PMMA_{65k}, PS_{37k}-*b*-PMMA_{37k}, PS_{42k}-*b*-PMMA_{16k}) were purchased from Polymer Source, Inc. BCP films were prepared by spin coating from 2 and 6 wt % toluene solutions (to prepare the films of different thicknesses) onto clean silicon substrates with native silicon dioxide films and with ALD-deposited 5 nm alumina adhesion layers. Samples demonstrating antireflection properties were prepared on clean glass substrates. In the case of the glass samples, no adhesion layer was necessary for producing a uniform antireflective coatings. Cleaning of the substrates was performed as following: 20 min of sonication in acetone, followed by 20 min of sonication in isopropanol, followed by 30 min of UV ozone exposure. After BCP deposition, the samples were kept on a hot plate at 180 °C for 10 min to evaporate residual toluene and to induce microphase separation. The thicknesses of resulting polymer films varied from 70 ± 5 nm to 400 ± 12 nm for 2 and 6 wt % toluene solutions, respectively.

Sequential infiltration synthesis reactants such as trimethyl aluminum ($\text{Al}(\text{CH}_3)_3$, TMA 96%) were purchased from Sigma-Aldrich and used as received. Deionized water was used in the deposition process.

Polymer Swelling. Swelling of the polymer films to increase the film thickness and to introduce pores for rapid infiltration with metal oxide was performed by immersing the whole sample into pure ethanol, and the samples were kept at 55, 65, or 75 °C for 1 h. Upon completion, the samples were dried under nitrogen gas flow.

Sequential Infiltration Synthesis. SIS was performed using GEMStar Thermal ALD system. The Al_2O_3 coatings were produced by infiltrating the polymer films using binary reactions of TMA/ H_2O . Exposure of BCP films to TMA vapor results in selective binding to polar groups in microphase separated polymer domains. Selectively bound $\text{Al}-(\text{CH}_3)_2$ reacts with water molecules in the subsequent SIS half-cycle. The SIS was performed at 90 °C (below the polymer glass transition temperatures) to avoid the flow of swelling-formed predefined polymer structures. All precursors were introduced into the reactor as room temperature vapors. Silicon or glass substrates with polymer films were loaded on a stainless steel tray and kept in a 200 sccm nitrogen flow for at least 30 min prior to deposition. One cycle of SIS was performed as follows: 10 mTorr of the synthesis reactant precursor was admitted into the reactor for 400 s. After that, the excess of the reactant was evacuated and followed by admitting 10 mTorr of H_2O for 120 s; the chamber was then purged with 200 sccm of nitrogen to remove not-infiltrated byproducts. The cycle was repeated several times to grow films of different porosity.

Thermal Annealing of the Polymers. Following SIS, the polymer component of the resulting film was removed by baking the samples in a Thermo Fisher Scientific tube furnace at 450 °C for 1 h while flowing oxygen gas at 50 sccm. Upon cooling, near-complete removal of carbon was confirmed with energy dispersive X-ray spectroscopy analysis of the film.

Characterization. Scanning electron microscopy (SEM) images were obtained using a FEI Nova 600 Nanolab dual-beam microscope with EDX capabilities. Spectroscopic ellipsometry (Horiba Uvisel Ellipsometer) was used to evaluate the film thickness and porosity. Specular reflectivity of the samples prepared on a glass substrate was measured with a Filmetrics F40 thin-film analyzer. SAXS and GISAXS data were collected at beamline 12-ID-B at Advanced Photon Source (APS). The transmittance of the samples was characterized using UV-vis spectrophotometer Cary-50. A 14 keV X-ray beam was exposed to thin-film samples using both transmission and grazing incidence reflection modes for SAXS and GISAXS measurements, respectively. The scattering data are collected with a Pilatus 2 M detector located

522 about 2 m away from samples. The contact angle measurements were
523 conducted using a Krüss DSA100 drop shape analyzer.

524 ASSOCIATED CONTENT

525 Supporting Information

526 The Supporting Information is available free of charge on the
527 ACS Publications website at DOI: [10.1021/acsnano.6b08361](https://doi.org/10.1021/acsnano.6b08361).

528 SEM image demonstrating the rupture of aluminum
529 oxide films during oxygen plasma-assisted polymer
530 removal. EDS analysis on Al_2O_3 film obtained by
531 thermally annealing of SIS sample ([PDF](#))

532 AUTHOR INFORMATION

533 Corresponding Authors

534 *E-mail: Diana.Berman@unt.edu.

535 *E-mail: eshevchenko@anl.gov.

536 ORCID

537 Byeongdu Lee: [0000-0003-2514-8805](https://orcid.org/0000-0003-2514-8805)

538 Elena V. Shevchenko: [0000-0002-5565-2060](https://orcid.org/0000-0002-5565-2060)

539 Notes

540 The authors declare no competing financial interest.

541 ACKNOWLEDGMENTS

542 Work at the Center for Nanoscale Materials, Advanced Photon
543 Source, and Electron Microscopy Center was supported by the
544 U.S. Department of Energy, Office of Science, Office of Basic
545 Energy Sciences, under contract no. DE-AC0206CH-11357.
546 The authors thank Dr. Leonidas Ocola for fruitful discussions
547 and help with the ALD/SIS instrument. The authors
548 acknowledge Dr. Gary Wiederrecht, Dr. Richard Schaller, Dr.
549 Xuedan Ma, Dr. David Gosztola, and Dr. John Harvey for
550 helpful discussions on optical properties of antireflective
551 coatings.

552 REFERENCES

- (1) Guldin, S.; Kohn, P.; Stefk, M.; Song, J.; Divitini, G.; Ecarla, F.; Ducati, C.; Wiesner, U.; Steiner, U. Self-Cleaning Antireflective Optical Coatings. *Nano Lett.* **2013**, *13*, 5329–5335.
- (2) Buskens, P.; Burghoorn, M.; Mourad, M. C. D.; Vroon, Z. Antireflective Coatings for Glass and Transparent Polymers. *Langmuir* **2016**, *32*, 6781–6793.
- (3) Raut, H. K.; Ganesh, V. A.; Nair, A. S.; Ramakrishna, S. Antireflective Coatings: A Critical, In-Depth Review. *Energy Environ. Sci.* **2011**, *4*, 3779–3804.
- (4) Woodhead Publishing Series in Electronic and Optical Materials. In *Optical Thin Films and Coatings*; Piegray, A., Flory, F., Eds. Woodhead Publishing: Cambridge, U.K., 2013.
- (5) Xi, J. Q.; Kim, J. K.; Schubert, E. F. Silica Nanorod-Array Films with Very Low Refractive Indices. *Nano Lett.* **2005**, *5*, 1385–1387.
- (6) Dodge, M. J. Refractive Properties of Magnesium Fluoride. *Appl. Opt.* **1984**, *23*, 1980–1985.
- (7) Xi, J. Q.; Schubert, M. F.; Kim, J. K.; Schubert, E. F.; Chen, M. F.; Lin, S. Y.; Liu, W.; Smart, J. A. Optical Thin-Film Materials with Low Refractive Index for Broadband Elimination of Fresnel Reflection. *Nat. Photonics* **2007**, *1*, 176–179.
- (8) Zou, L. P.; Li, X. G.; Zhang, Q. H.; Shen, J. An Abrasion-Resistant and Broadband Antireflective Silica Coating by Block Copolymer Assisted Sol-Gel Method. *Langmuir* **2014**, *30*, 10481–10486.
- (9) Hiller, J.; Mendelsohn, J. D.; Rubner, M. F. Reversibly Erasable Nanoporous Anti-Reflection Coatings from Polyelectrolyte Multi-layers. *Nat. Mater.* **2002**, *1*, 59–63.

- (10) Li, Y.; Liu, F.; Sun, J. Q. A Facile Layer-by-Layer Deposition Process for the Fabrication of Highly Transparent Superhydrophobic Coatings. *Chem. Commun.* **2009**, 2730–2732.
- (11) Burghoorn, M.; Roosen-Melsen, D.; de Riet, J.; Sabik, S.; Vroon, Z.; Yakimets, I.; Buskens, P. Single Layer Broadband Anti-Reflective Coatings for Plastic Substrates Produced by Full Wafer and Roll-to-Roll Step-and-Flash Nano-Imprint Lithography. *Materials* **2013**, *6*, 3710–3726.
- (12) Leem, J. W.; Yu, J. S. Wafer-Scale Highly-Transparent and Superhydrophobic Sapphires for High Performance Optics. *Opt. Express* **2012**, *20*, 26160–26166.
- (13) Ye, X.; Huang, J.; Geng, F.; Liu, H.; Sun, L.; Yan, L.; Jiang, X.; Wu, W.; Zheng, W. High Power Laser Antireflection Subwavelength Grating on Fused Silica by Colloidal Lithography. *J. Phys. D: Appl. Phys.* **2016**, *49*, 265104.
- (14) Ye, X.; Jiang, X.; Huang, J.; Geng, F.; Sun, L.; Zu, X.; Wu, W.; Zheng, W. Formation of Broadband Antireflective and Superhydrophilic Subwavelength Structures on Fused Silica Using OneStep Self-Masking Reactive Ion Etching. *Sci. Rep.* **2015**, *5*, 13023.
- (15) Stefk, M.; Guldin, S.; Vignolini, S.; Wiesner, U.; Steiner, U. Block Copolymer Self-Assembly for Nanophotonics. *Chem. Soc. Rev.* **2015**, *44*, 5076–5091.
- (16) Blumstein, A. Polymerization of Adsorbed Monolayers. II. Thermal Degradation of the Inserted Polymer. *J. Polym. Sci., Part A: Gen. Pap.* **1965**, *3*, 2665–2672.
- (17) Prevo, B. G.; Hwang, Y.; Velev, O. D. Convective Assembly of Antireflective Silica Coatings with Controlled Thickness and Refractive Index. *Chem. Mater.* **2005**, *17*, 3642–3651.
- (18) Kennedy, S. R.; Brett, M. J. Porous Broadband Antireflection Coating by Glancing Angle Deposition. *Appl. Opt.* **2003**, *42*, 4573–4579.
- (19) Biswas, M.; Libera, J. A.; Darling, S. B.; Elam, J. W. New Insight into the Mechanism of Sequential Infiltration Synthesis from Infrared Spectroscopy. *Chem. Mater.* **2014**, *26*, 6135–6141.
- (20) Peng, Q.; Tseng, Y. C.; Darling, S. B.; Elam, J. W. Nanoscopic Patterned Materials with Tunable Dimensions via Atomic Layer Deposition on Block Copolymers. *Adv. Mater.* **2010**, *22*, 5129–5133.
- (21) Peng, Q.; Tseng, Y. C.; Darling, S. B.; Elam, J. W. A Route to Nanoscopic Materials via Sequential Infiltration Synthesis on Block Copolymer Templates. *ACS Nano* **2011**, *5*, 4600–4606.
- (22) Tseng, Y.-C.; Peng, Q.; Ocola, L. E.; Czaplewski, D. A.; Elam, J. W.; Darling, S. B. Etch Properties of Resists Modified by Sequential Infiltration Synthesis. *J. Vac. Sci. Technol., B: Nanotechnol. Microelectron.: Mater., Process., Meas., Phenom.* **2011**, *29*, 06FG01.
- (23) Tseng, Y.-C.; Peng, Q.; Ocola, L. E.; Elam, J. W.; Darling, S. B. Enhanced Block Copolymer Lithography Using Sequential Infiltration Synthesis. *J. Phys. Chem. C* **2011**, *115*, 17725–17729.
- (24) Black, C. T.; Ruiz, R.; Breyta, G.; Cheng, J. Y.; Colburn, M. E.; Guarini, K. W.; Kim, H. C.; Zhang, Y. Polymer Self Assembly in Semiconductor Microelectronics. *IBM J. Res. Dev.* **2007**, *51*, 605–633.
- (25) Checco, A.; Rahman, A.; Black, C. T. Robust Superhydrophobicity in Large-Area Nanostructured Surfaces Defined by Block-Copolymer Self Assembly. *Adv. Mater.* **2014**, *26*, 886–891.
- (26) Ruiz, R.; Kang, H.; Detcherry, F. A.; Dobisz, E.; Kercher, D. S.; Albrecht, T. R.; de Pablo, J. J.; Nealey, P. F. Density Multiplication and Improved Lithography by Directed Block Copolymer Assembly. *Science* **2008**, *321*, 936–939.
- (27) Biswas, M.; Libera, J. A.; Darling, S. B.; Elam, J. W. Kinetics for the Sequential Infiltration Synthesis of Alumina in Poly(methyl methacrylate): An Infrared Spectroscopic Study. *J. Phys. Chem. C* **2015**, *119*, 14585–14592.
- (28) Kim, H. C.; Park, S. M.; Hinsberg, W. D. Block Copolymer Based Nanostructures: Materials, Processes, and Applications to Electronics. *Chem. Rev.* **2010**, *110*, 146–177.
- (29) Bang, J.; Jeong, U.; Ryu, D. Y.; Russell, T. P.; Hawker, C. J. Block Copolymer Nanolithography: Translation of Molecular Level Control to Nanoscale Patterns. *Adv. Mater.* **2009**, *21*, 4769–4792.

647 (30) Groner, M. D.; Fabreguette, F. H.; Elam, J. W.; George, S. M.
648 Low-Temperature Al₂O₃ Atomic Layer Deposition. *Chem. Mater.*
649 **2004**, *16*, 639–645.

650 (31) Wang, Y. Nondestructive Creation of Ordered Nanopores by
651 Selective Swelling of Block Copolymers: Toward Homoporous
652 Membranes. *Acc. Chem. Res.* **2016**, *49*, 1401–1408.

653 (32) Yin, J.; Yao, X.; Liou, J.-Y.; Sun, W.; Sun, Y.-S.; Wang, Y.
654 Membranes with Highly Ordered Straight Nanopores by Selective
655 Swelling of Fast Perpendicularly Aligned Block Copolymers. *ACS*
656 *Nano* **2013**, *7*, 9961–9974.

657 (33) Lee, B.; Yoon, J.; Oh, W.; Hwang, Y.; Heo, K.; Jin, K. S.; Kim, J.;
658 Kim, K. W.; Ree, M. In-situ Grazing Incidence Small-Angle X-ray
659 Scattering Studies on Nanopore Evolution in Low-k Organosilicate
660 Dielectric Thin Films. *Macromolecules* **2005**, *38*, 3395–3405.

661 (34) Lee, B. D.; Park, Y. H.; Hwang, Y. T.; Oh, W.; Yoon, J.; Ree, M.
662 Ultralow-k Nanoporous Organosilicate Dielectric Films Imprinted
663 with Dendritic Spheres. *Nat. Mater.* **2005**, *4*, 147–151.

664 (35) Elam, J. W.; Routkevitch, D.; Mardilovich, P. P.; George, S. M.
665 Conformal Coating on Ultrahigh-Aspect-Ratio Nanopores of Anodic
666 Alumina by Atomic Layer Deposition. *Chem. Mater.* **2003**, *15*, 3507–
667 3517.

668 (36) Rywak, A. A.; Burlitch, J. M. Sol–Gel Synthesis of Nanocrystal-
669 line Magnesium Fluoride: Its Use in the Preparation of MgF₂ Films
670 and MgF₂–SiO₂ Composites. *Chem. Mater.* **1996**, *8*, 60–67.

671 (37) Dobrowolski, J. A.; Guo, Y. N.; Tiwald, T.; Ma, P. H.; Poitras,
672 D. Toward Perfect Antireflection Coatings. 3. Experimental Results
673 Obtained with the Use of Reststrahlen Materials. *Appl. Opt.* **2006**, *45*,
674 1555–1562.

675 (38) Dobrowolski, J. A.; Poitras, D.; Ma, P.; Vakil, H.; Acree, M.
676 Toward Perfect Antireflection Coatings: Numerical Investigation.
677 *Appl. Opt.* **2002**, *41*, 3075–3083.

678 (39) Poitras, D.; Dobrowolski, J. A. Toward Perfect aAntireflection
679 Coatings. 2. Theory. *Appl. Opt.* **2004**, *43*, 1286–1295.